Debonding criterion based on the intensity of singular stress

Proceedings of the 2nd International Symposium on
Engineering Mechanics and its Applications, pp. 105-111, 2013

DEBONDING CRITERION BASED ON THE INTENSITY OF SINGULAR STRESS

Tatsujiro MIYAZAKI[1], Nao-Aki NODA[2], Long LI[3],

Takumi UCHIKOBA[3] and Yoshikazu SANO[2]

[1] University of the Ryukyus, Okinawa, Japan
[2] Kyushu Institute of Technology, Fukuoka, Japan
[3]Graduate School of Engineering, Kyushu Institute of Technology, Fukuoka, Japan

Abstract: In the previous study, the authors discussed a debonding fracture criterion for single lap joints (SLJs) with varying the adhesive thickness and overlap length in terms of the critical intensity of a singular stress field. Here it is simply assumed that the identical singular stress fields are formed at the edge corner of the SLJ for different geometries. In this paper, by applying the reciprocal work contour integral method (RWCIM) it is shown that the two distinct intensities of the singular stress fields are determined accurately when the orders of stress singularity are two different real numbers. It is found that the ratio of the intensities of two types of the singular stress fields is almost the same for the wide range of the adhesive thickness and the overlap length. Then, it is found that the debonding fracture criterion is represented in terms of the intensity of the singular stress field with the strong stress singularity when aluminum alloy is bonded by epoxy resin.

Keywords: Intensity Of Singular Stress Field, Adhesion, Interface, Single Lap Joint, Reciprocal Work Contour Integral Method, Finite Element Method.

1 INTRODUCTION

The testing method for the tensile lap-shear strength of the single lap joint (SLJ) is standardized by Japanese Industrial Standards (JIS) [1]. In this standard, the fracture tensile load is measured as the tensile lap-shear strength. Therefore, when the overlap length and adhesive thickness are different, the tensile lap-shear strength is also changed even if the same adherend and adhesive are used. The mechanical parameter, which is suitable for the design, should be chosen as the tensile lap-shear strength from the viewpoint of the fracture phenomenon.

Recently, Mintzas – Nowell [2] reported that the debonding fracture criterion for the adhesively bonded joints can be expressed with the critical value of the generalised stress intensity factor, H_{cr} [2 - 4]. The authors also confirmed that the debonding fracture criterion for the butt joints with the various adhesive thicknesses can be expressed with the critical intensity of the singular stress field at the fracture [5]. The singular stress field of the butt joints is expressed with only one singular stress term with order $\lambda-1$. However, generally, the singular stress field which is formed near an arbitrary interface corner edge is expressed with several singular stress terms with the orders λ_1-1, λ_2-1, $\cdots$. Because the intensities of the singular stress field the number of which equals that of the orders exit, it is difficult to evaluate the debonding fracture criterion base on the intensity of the singular stress field. The authors clarified that the singular stress fields of the SLJs with various overlap lengths and adhesive thicknesses are almost similar by FEM analyses based on the crack tip stress method [6, 7] when the singular stress field of the SLJ is often expressed with two singular stress terms with the real orders λ_1-1 and λ_2-1 ($\lambda_1<\lambda_2$). From the analysis results, the debonding fracture criterion of the SLJs can be expressed with the critical intensity of the singular stress field at the fracture. However, the intensities of the singular stress field were not calculated in the earlier study [6, 7]. The similarity of the singular stress field needs to be examined from the intensities of the singular stress field in detail.

In this study, the intensities of the singular stress field of the SLJ with two real orders λ_1-1 and λ_2-1 ($\lambda_1<\lambda_2$) are calculated by the reciprocal work contour integral method (RWCIM) [8] exactly. The similarity

of the singular stress field is examined from the intensities of the singular stress field. The validity that the debonding fracture criterion of the SLJs can be expressed with $K_{\sigma c} = \text{constant}$ is discussed, where $K_{\sigma c}$ is the critical intensity of the singular stress field at the fracture.

2 EXPERIMENTAL DATA

The tensile shear-lap strength as obtained from experiments performed by Park et al [9] is used. Figure 1 shows the schematic illustration of the specimens. In the experiment, the adherend and adhesive are aluminum alloy 6061-T6 (Young's modulus $E_1 = 68.9$ GPa, Poisson's ratio $\nu_1 = 0.3$) and epoxy resin ($E_2 = 4.2$ GPa, $\nu_2 = 0.45$), respectively. The total length of the specimen is 225 mm; the adhesive thickness is varied from 0.15 mm to 0.9 mm; the overlap length is vaired from 15 mm to 50 mm.

Table 1 shows the tensile lap-shear strength P_{af}. In the experiment, the linear relation between the load and displacement was obtained except for the specimen A10. The results suggest that the fracture was caused by the debonding crack which was initiated from the corner edge of the interface between the adhesive and the adherend. Then, the experimental result gives the validity that the critical intensity of the singular stress field at the fracture is used as the debonding fracture criterion.

Figure 2 shows the tensile lap-shear strength P_{af} under t_2 constant condition. The P_{af} tends to increase with increasing the l_2. Figure 3 shows the average shear stress at the fracture, $\tau_c = P_{af}/(l_2 W)$. When the l_2 is smaller than 15 mm, the τ_c becomes constant at about 28.7 MPa. However, When the l_2 is larger than 15 mm, the τ_c tends to decrease. Nono and Nagahiro [10] reported that the fracture is caused by the general yielding of the adhesive layer and the τ_c becomes constant when the overlap length is short. In this study, it is supposed that debonding fracture occurs when $l_2 > 15$ mm.

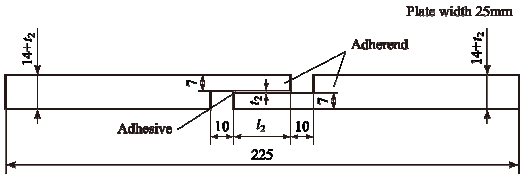

Fig. 1. Specimen configurations [9].

Table 1. Experimental results [9].

(a) t_2 constant condition

Specimen	l_2 [mm]	t_2 [mm]	P_{af} [kN]
A10	10	0.15	6.87
A15	15	0.15	10.57
A20	20	0.15	12.41
A25	25	0.15	14.17
A30	30	0.15	14.56
A35	35	0.15	16.41
A40	40	0.15	18.09
A50	50	0.15	18.22

(b) l_2 constant condition

Specimen	l_2 [mm]	t_2 [mm]	P_{af} [kN]
A25	25	0.15	14.17
A25-30	25	0.30	14.32
A25-45	25	0.45	14.26
A25-90	25	0.90	14.19
A30	30	0.15	14.56
A30-30	30	0.30	16.91
A30-45	30	0.45	16.12
A30-90	30	0.90	15.37

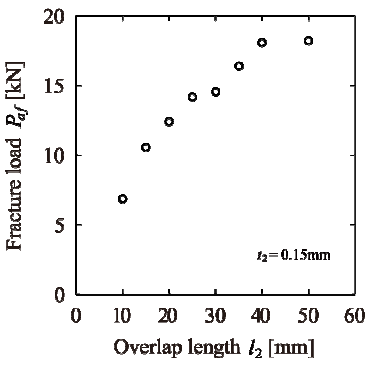

Fig. 2. Adhesive tensile strength of specimens with $t_2 = 0.15$ mm [9].

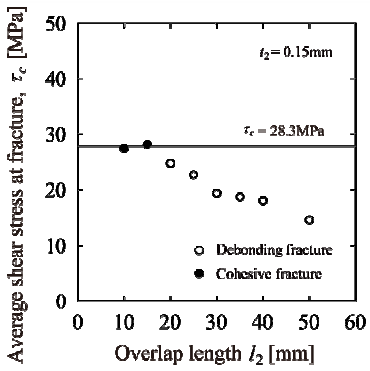

Fig. 3. Average shear stress at fracture of specimens with $t_2 = 0.15$ mm [9].

3 SINGULAR STRESS FIELD

3.1 Characteristics of the singular stress field

Figure 4 shows the schematic illustration of the analysis model and boundary condition. l_1 and t_1 are adherend length and adherend thickness, respectively; l_2 and t_2 are overlap length and adhesive thickness, respectively; E is Young's modulus, ν is Poisson's ratio, and subscripts 1 and 2 refer to the adherend and the adhesive, respectively.

The singular stress field is formed at the corner edge of the interface between the adherend and the adhesive. The singular stress field is governed by the order of stress singularity, $\lambda-1$. The eigenvalue λ can be obtained by solving the eigenequation which was derived by Bogy [11]. In the case of the corner edge as shown in Fig. 4, the eigenequation is given by the following equation [6, 7, 11].

$$\begin{aligned} &4\sin^2(\pi\lambda)\left\{\sin^2\left(\frac{\pi\lambda}{2}\right)-\lambda^2\right\}\beta^2+4\lambda^2\sin^2(\pi\lambda)\alpha\beta+\left\{\sin^2\left(\frac{\pi\lambda}{2}\right)-\lambda^2\right\}\alpha^2 \\ &-4\lambda^2\sin^2(\pi\lambda)\beta-2\left\{\lambda^2\cos(2\pi\lambda)+\sin^2\left(\frac{\pi\lambda}{2}\right)\cos(\pi\lambda)+\frac{1}{2}\sin^2(\pi\lambda)\right\}\alpha+\sin^2\left(\frac{3\pi}{2}\lambda\right)-\lambda^2=0 \end{aligned} \tag{1}$$

Here, α and β are Dundurs' parameter [12] and defined as follows

$$\alpha=\frac{G_2(\kappa_1+1)-G_1(\kappa_2+1)}{G_2(\kappa_1+1)+G_1(\kappa_2+1)},\ \beta=\frac{G_2(\kappa_1-1)-G_1(\kappa_2-1)}{G_2(\kappa_1+1)+G_1(\kappa_2+1)},\ \kappa_m=\frac{3-\nu_m}{1+\nu_m}(\text{plain stress}),\ 3-4\nu_m(\text{plain strain}) \tag{2}$$

Here, G_m ($m=1,2$) is the shear modulus of elasticity.

The root of the eigenequation (1), λ, depends on the α and the β. In the case of the material combination in Section 2, $\lambda_1=0.6062$ and $\lambda_2=0.9989$ are obtained from $\alpha=-0.8699$ and $\beta=-0.006642$. The stresses at a radial distance r from the point O on the interface, σ_θ and $\tau_{r\theta}$, are expressed as follows.

$$\sigma_\theta=\frac{K_1}{r^{1-\lambda_1}}f_{\theta\theta}(0,\lambda_1)+\frac{K_2}{r^{1-\lambda_2}}f_{\theta\theta}(0,\lambda_2)=\frac{K_{\sigma,\lambda_1}}{r^{1-\lambda_1}}+\frac{K_{\sigma,\lambda_2}}{r^{1-\lambda_2}},\ \tau_{r\theta}=\frac{K_1}{r^{1-\lambda_1}}f_{r\theta}(0,\lambda_1)+\frac{K_2}{r^{1-\lambda_2}}f_{r\theta}(0,\lambda_2)=\frac{K_{\tau,\lambda_1}}{r^{1-\lambda_1}}+\frac{K_{\tau,\lambda_2}}{r^{1-\lambda_2}} \tag{3}$$

Here, K_1 and K_2 are real numbers, $f_{\theta\theta}(\theta,\lambda_k)$ and $f_{r\theta}(\theta,\lambda_k)$ are non-dimensional funuctions of the angle θ, the λ_k, the α and the β, K_{σ,λ_k} and K_{τ,λ_k} are the intensities of the singular stress field. Because four intensities of the singular stress field, K_{σ,λ_1}, K_{σ,λ_2}, K_{τ,λ_1} and K_{τ,λ_2} are determined by two real numbers K_1 and K_2, the singular stress field in the vicinity of the corner edge is also determined by them.

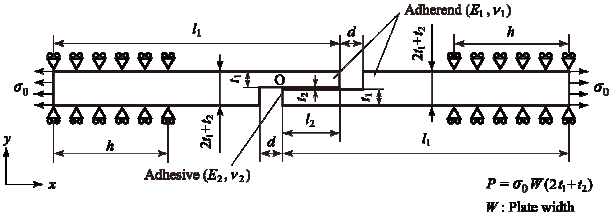

Fig. 4. Analysis model and boundary condition.

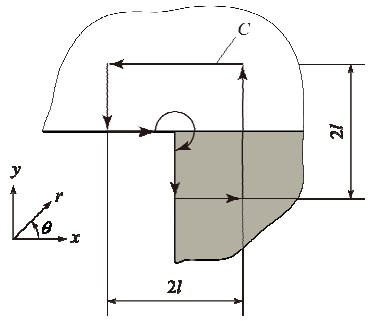

Fig. 5. Contour integral path for RWCIM.

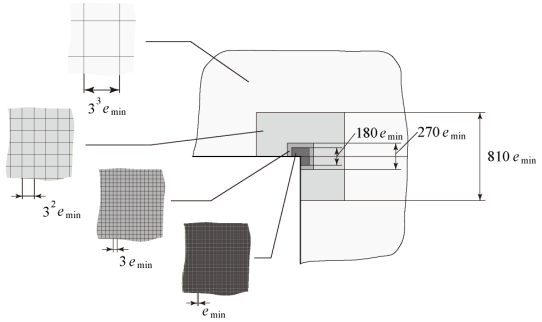

Fig. 6. Mesh pattern near the interface edge corner.

3.2 Analysis method

The intensities of the singular stress field, K_{σ,λ_k} and K_{τ,λ_k}, were calculated by RWCIM. Figure 5 shows the integral path C. The linear elastic analyses were perfomed under the plane strain condition using the commercial FEM code MSC Marc 2008 R1. Figure 6 shows the schematic illustration of the mesh pattern in the vicinity of the interface corner edge. In the region which contains the corner edge and the integral path, 8-Node quadratic isoparametric element was used; in the other region, 4-Node quadratic isoparametric element was used.

3.3 Analysis results and discussion

The analysis result of the specimen A25 is mentioned. The contour integral path C in Fig. 5 and the mesh pattern in Fig. 6 were used in order to calculate the intensities of the singular stress field. The intensities of the singular stress field under $\sigma_0 = 1$ MPa were calculated changing the $e_{\min}$ and the $l/e_{\min}$ variously. Table 2 shows the intensities of the singular stress field. The K_{σ,λ_1} value converges at 0.1010 when $l/e_{\min} \geq 10$. On the other hand, the K_{σ,λ_2} value tends to converge at -0.5485 with increasing the $l/e_{\min}$. When $\sigma_0 = 1$ MPa, $K_{\sigma,\lambda_1} = 0.1010$ MPa$\cdot$m$^{1-\lambda_1}$, $K_{\tau,\lambda_1} = -0.04723$ MPa$\cdot$m$^{1-\lambda_1}$, $K_{\sigma,\lambda_2} = -0.5485$ MPa$\cdot$m$^{1-\lambda_2}$ and $K_{\tau,\lambda_2} = -0.01168$ MPa$\cdot$m$^{1-\lambda_2}$ were obtained in this analysis. Figure 7 shows the stress distributions on the interface. The solid line is the stresses σ_θ and $\tau_{r\theta}$ which are obtained by substituting these intensities of the singular stress field into Eq. 3. Then, the circle and triangle marks are the stresses σ_θ and $\tau_{r\theta}$ by FEM, respectively. When $r \leq 0.01$ mm, the marks are good agreement with the solid curves.

Table 3 shows the intensities of the singular stress field of all specimens. Because the K_{σ,λ_1} and the K_{τ,λ_1} are determined by the K_1 as shown in Eq. 3, the $K_{\tau,\lambda_1}/K_{\sigma,\lambda_1}$ becomes constant independent of the l_2 and the t_2. In the present SLJ models, $K_{\tau,\lambda_1}/K_{\sigma,\lambda_1} = -0.4678$ and $K_{\tau,\lambda_2}/K_{\sigma,\lambda_2} = 0.02130$ were obtained. Then, the $K_{\sigma,\lambda_2}/K_{\sigma,\lambda_1}$ values and the $K_{\tau,\lambda_2}/K_{\tau,\lambda_1}$ values of all the models except for the models A10 and A15 range from -5.574 to -4.827 and from 0.2198 to 0.2538, respectively. Figure 8 shows the relation between $\sigma_\theta/(K_{\sigma,\lambda_1}/r^{1-\lambda_1})$, $\tau_{r\theta}/(K_{\tau,\lambda_1}/r^{1-\lambda_1})$ and r. The dashed lines are the $\sigma_\theta/(K_{\sigma,\lambda_1}/r^{1-\lambda_1})$ and the $\tau_{r\theta}/(K_{\tau,\lambda_1}/r^{1-\lambda_1})$ of the model A50 the $K_{\sigma,\lambda_2}/K_{\sigma,\lambda_1}$ and the $K_{\tau,\lambda_2}/K_{\tau,\lambda_1}$ of which are mininum; the chain lines are the $\sigma_\theta/(K_{\sigma,\lambda_1}/r^{1-\lambda_1})$ and the $\tau_{r\theta}/(K_{\tau,\lambda_1}/r^{1-\lambda_1})$ of the model A25-90 the $K_{\sigma,\lambda_2}/K_{\sigma,\lambda_1}$ and the $K_{\tau,\lambda_2}/K_{\tau,\lambda_1}$ of which are maximum. There are a few differences between the dashed line and the chain line. From the analysis results, it can be found that the singular stress fields of all the models except for the models A10 and A15 are similar. Then, the σ_θ and the $\tau_{r\theta}$ are approximately expressed with the following equation.

$$\sigma_\theta \cong \frac{K_{\sigma,\lambda_1}}{r^{1-\lambda_1}}\left(1 + C_\sigma r^{\lambda_2-\lambda_1}\right),\ \tau_{r\theta} \cong \frac{K_{\tau,\lambda_1}}{r^{1-\lambda_1}}\left(1 + C_\tau r^{\lambda_2-\lambda_1}\right) \tag{4}$$

Here, C_σ and C_τ are constant.

Because the K_{σ,λ_1} and the K_{τ,λ_1} are determined by the K_1 as shown in Eq. 3, the intensities of the singular stress field can be represented with the K_{σ,λ_1}. Therefore, the condition that the debonding fracture of the SLJ does not occur can be expressed with the following equation.

$$K_{\sigma,\lambda_1} \leq K_{\sigma c} \tag{5}$$

Here, $K_{\sigma c}$ is the critical intensity of the singular stress field at the fracture.

Table 2. K_{σ,λ_1} and K_{σ,λ_2} of specimen A25 under $\sigma_0 = 1$ MPa.

$l/e_{\min}$	$e_{\min} = 3^{-11}$ mm		$e_{\min} = 3^{-9}$ mm	
	K_{σ,λ_1}	K_{σ,λ_2}	K_{σ,λ_1}	K_{σ,λ_2}
5	0.1011	-0.5553	0.1011	-0.5510
10	0.1010	-0.5500	0.1010	-0.5491
20	0.1010	-0.5492	0.1010	-0.5486
40	0.1010	-0.5484	0.1010	-0.5486
80	0.1010	-0.5485	0.1010	-0.5484

K_{σ,λ_1} : MPa$\cdot$m$^{1-\lambda_1}$, K_{σ,λ_2} : MPa$\cdot$m$^{1-\lambda_2}$

Table 3. Intensities of singular stress field under $\sigma_0 = 1$ MPa.

(a) t_2 constant condition

Specimen	K_{σ,λ_1}	K_{σ,λ_2}	K_{τ,λ_1}	K_{τ,λ_2}
A10	0.1065	-0.6469	-0.04981	-0.01378
A15	0.1083	-0.6021	-0.05068	-0.01282
A20	0.1056	-0.5735	-0.04940	-0.01222
A25	0.1010	-0.5485	-0.04723	-0.01168
A30	0.09606	-0.5237	-0.04494	-0.01116
A35	0.09107	-0.4985	-0.04261	-0.01062
A40	0.08618	-0.4741	-0.04032	-0.01010
A50	0.07680	-0.4280	-0.03593	-0.009118

(b) l_2 constant condition

Specimen	K_{σ,λ_1}	K_{σ,λ_2}	K_{τ,λ_1}	K_{τ,λ_2}
A25	0.1010	-0.5485	-0.04723	-0.01168
A25-30	0.09796	-0.5022	-0.04583	-0.01070
A25-45	0.09777	-0.4884	-0.04574	-0.01040
A25-90	0.1013	-0.4888	-0.04738	-0.01041
A30	0.09606	-0.5237	-0.04494	-0.01116
A30-30	0.09294	-0.4785	-0.04348	-0.01019
A30-45	0.09246	-0.4644	-0.04325	-0.009893
A30-90	0.09482	-0.4631	-0.04436	-0.009865

K_{σ,λ_1}, K_{τ,λ_1} : MPa·m$^{1-\lambda_1}$, K_{σ,λ_2}, K_{τ,λ_2} : MPa·m$^{1-\lambda_2}$

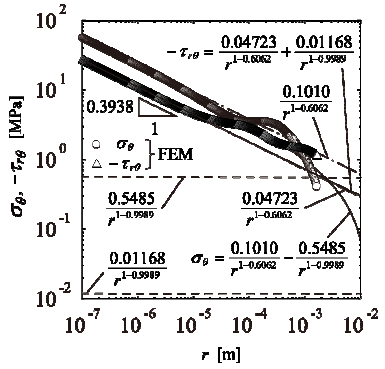

Fig. 7. Comparison between stress distribution of Specimen A 25 by Eq. 3 and FEM.

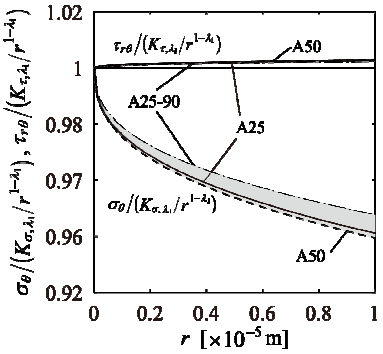

Fig. 8. Relationship between $\sigma_\theta/(K_{\sigma,\lambda_1}/r^{1-\lambda_1})$, $\tau_{r\theta}/(K_{\tau,\lambda_1}/r^{1-\lambda_1})$ and r.

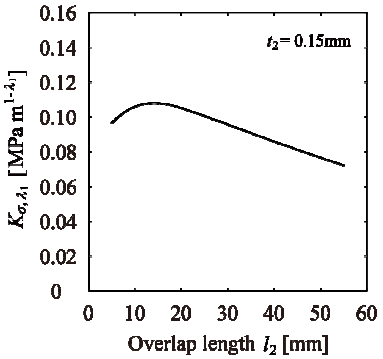

Fig. 9. Relationship between K_{σ,λ_1} and l_2.

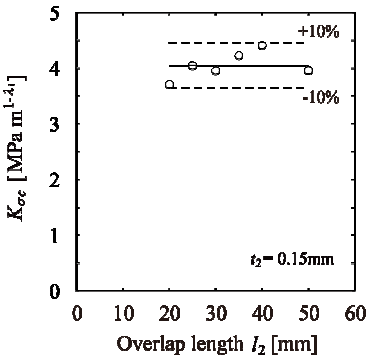

Fig. 10. Relationship between $K_{\sigma c} = K_{\sigma,\lambda_1}|_{P=P_{af}}$ and l_2

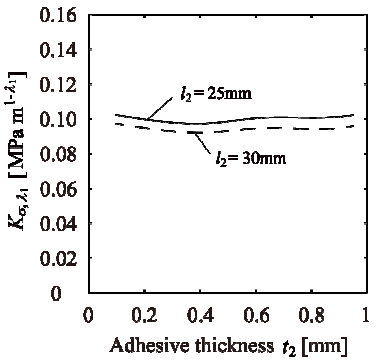

Fig. 11. Relationship between K_{σ,λ_1} and t_2.

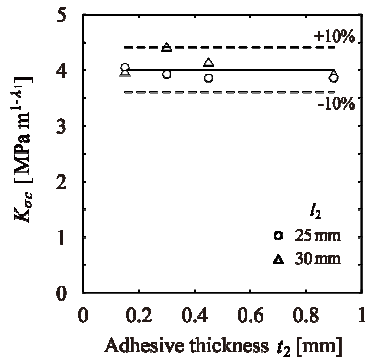

Fig. 12. Relationship between $K_{\sigma c} = K_{\sigma,\lambda_1}|_{P=P_{af}}$.

and t_2

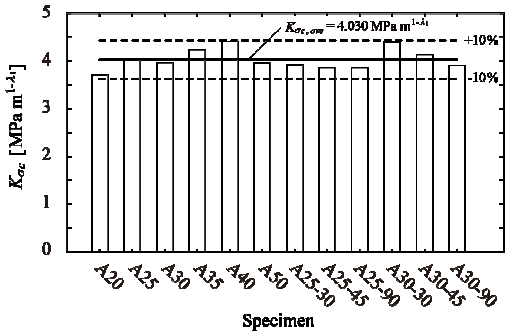

Fig. 13. Debonding fracture criterion $K_{\sigma c}$.

4 DEBONDING FRACTURE CRITERION

As mentioned in Section 3, the intensities of the singular stress field can be represented with the K_{σ,λ_1} from the similarity of the simgular stress field. Figure 9 shows the K_{σ,λ_1} values of the specimens with $t_2 = 0.15$ mm under $\sigma_0 = 1$ MPa. When $l_2 \geq 15$ mm, the K_{σ,λ_1} tends to decrease with increasing the l_2. Figure 10 shows the critical intensities of the singular stress field of specimen with $t_2 = 0.15$ mm, where $K_{\sigma,\lambda_1}|_{P=P_{af}}$ is the intensity of the singular stress field under $P = P_{af}$, $K_{\sigma c} = K_{\sigma,\lambda_1}|_{P=P_{af}}$. The $K_{\sigma c}$ values become constant independet of the l_2.

Figure 11 shows the K_{σ,λ_1} values of the specimens with $l_2 = 25$, 30 mm under $\sigma_0 = 1$ MPa. Figure 12 shows the critical intensities of the singular stress field of the specimen with $l_2 = 25$, 30 mm. The $K_{\sigma c}$ values become constant independet of the t_2.

Figure 13 shows the $K_{\sigma c}$ values of all specimens in Figs. 10 and 12. The solid line is the average of the $K_{\sigma c}$ values, $K_{\sigma c,ave}$. In this study, the $K_{\sigma c,ave}$ was 4.030 MPa$\cdot$m$^{1-\lambda_1}$. The $K_{\sigma c}$ values were within the range of 10 % difference. From the result, it can be confirmed that the $K_{\sigma c}$ becomes constant independent of the l_2 and the t_2.

5 CONCLUSION

In this study, four intensities of the singular stress field of the SLJ with the different real orders $\lambda_1 - 1$ and $\lambda_2 - 1$, K_{σ,λ_1}, K_{σ,λ_2}, K_{τ,λ_1} and K_{τ,λ_2}, were calculated by RWCIM exactly. Then, the similarity of the singular stress field and the debonding fracture criterion based on the intensity of the singular stress field were examined.

(1) The debonding fracture criterion was expressed with the critical intensity of the singular stress field at the fracture except that the overlap length is short significantly.

(2) The $K_{\sigma,\lambda_2}/K_{\sigma,\lambda_1}$ and $K_{\tau,\lambda_2}/K_{\tau,\lambda_1}$ are nearly equal independent of the overlap length l_2 and the adhesive thickness t_2. From the analysis results, it was found that the similar singular stress fields are formed even if the l_2 and the t_2 are different.

(3) Four intensities of the singular stress field can be represented with the K_{σ,λ_1} based on the similarity of the singular stress field. Therefore, the debonding fracture criterion $K_{\sigma c}$ was expressed with the critical intensity of the singular stress field at the fracture, $K_{\sigma,\lambda_1}|_{P=P_{af}}$, within the range of 10% error.

REFERENCES

[1] JIS K6850, Adhesives-Determination of tensile lap-shear strength or rigid-to-rigid bonding assemblies.

[2] A. Mintzas & D. Nowell, Engineering Fracture Mechanics, 80 (2012), 13 - 27.

[3] Z. Qian & A. R. Akisanya, Acta Materialia, 46 - 14(1998), 4895 - 4904.

[4] A. R. Akisanya & C. S. Meng, Journal of the Mechanics and Physics of Solids, 51 (2003), 27 - 46.

[5] N. -A. Noda et al., Proc. 3rd ACMFMS, (2012), 813-816.

[6] N. -A. Noda et al., Trans. JSME, A78 – 789 (2012), 651 – 655.

[7] T. Miyazaki et al., Trans. JIEP, 16 – 2 (2012), 813 – 316.

[8] W. C. Carpenter & C. Byers : International Journal of Fracture, **35**, (1987), pp. 245-268.

[9] J. -H. Park, J. -H. Choi, J. -H. Kweon : Composite Structures, **92** (2010), 2226-2235.

[10] K. Nono & T. Nagahiro, Trans. JSME, A52 – 479 (1986), 1698 – 1707.

[11] D. B. Bogy : Transaction of the ASME, Journal of Applied Mechanics, **35**, (1968), 460-466.

[12] J. Dundurs : Journal of Applied Mechanics, **36**, (1969), 650-652.